The effect of copper loading on iron carbide formation and surface species in iron-based Fischer-Tropsch synthesis catalysts

Diego Peña,[a] Lise Jensen,[a] Andrea Cognigni,[a] Rune Myrstad,[b] Thomas Neumayer,[a] Wouter van Beek,[c] and Magnus Rønning*[a]

[a]	Dr. D. Peña, L. Jensen, T. Neumayer, Dr. A. Cognigni, Prof. M. Rønning
	Department of Chemical Engineering
	Norwegian University of Science and Technology
	7491 Trondheim (Norway)
	E-mail: magnus.ronning@ntnu.no
[b]	Dr. M. Myrstad
	SINTEF, Materials and Chemistry
	7465 Trondheim (Norway)
[c]	Dr. W. van Beek
	The Swiss-Norwegian Beamlines at ESRF
	BP 220, F-38043 Grenoble (France)

Abstract:

The effect of copper as promoter on iron carbide formation and the nature of surface species on iron-based catalyst during Fischer–Tropsch synthesis (FTS) have been investigated. Iron-based catalysts (15 wt% of Fe) supported on alumina promoted with copper (0, 0.6, 2 and 5 wt%) were characterised in situ at relevant FTS conditions. The catalysts promoted with 2 and 5 wt% of Cu showed higher catalytic activity due to the formation of Hägg carbide (Fe_5C_2) detected by in situ XANES and XRD. The carbide formation is attributed to a weakening of the iron-alumina mixed-compound interactions, and hence increasing iron reducibility and dispersion. The in situ XANES measurements indicated a maximum carburization degree ($\sim$ 20-22 %) even at high Cu loading. The catalyst promoted with 5 wt% of Cu exhibited higher water-gas shift activity. Aliphatic hydrocarbons, formate and carboxylate species were detected on the catalyst surface during FTS. After exposing the spent catalysts to hydrogenation conditions, the carboxylate species remained strongly adsorbed while aliphatic hydrocarbons and formate species disappeared. The accumulation of oxygenates species on the catalyst surface increased with Cu loading. The interaction of oxygenates with alumina and iron oxide particles (Fe_xO_y) were revealed, with the latter being a possible reason for inhibition of further iron carburization.

Introduction

Fischer-Tropsch synthesis is an established industrial technology forming part of the coal-to-liquids (CTL), gas-to-liquids (GTL) and biomass-to-liquids (BTL), collectively known as XTL processes which convert syngas (CO and H2) into synthetic hydrocarbons and chemicals using mainly iron-based and cobalt-based catalysts.[1,2] Typical industrial-scale XTL plants have capacities of hundreds of thousands barrels per day (bpd).[3] New modular small FTS installations in the 100-1000 bpd range are in the near-term driven by regulations prohibiting flaring of associated-gas and in the medium-term by the desire to generate fuels and chemicals from biomass.[4,5] For these FTS installations, there are several challenges; firstly the compact reactor and simplified process configurations do not offer the tight control of temperature and gas purity as for industrial-scale XTL plants.[6–8] Secondly, the syngas feed from gasified biomass may be rich in CO2 with a fluctuating syngas ratio, although operating the FTS unit with a CO2 rich feed without purification could result in a simpler and lower cost process.[4,9]

Fe catalysts are attractive particularly because of their capacity to manage different syngas ratios, water gas shift (WGS) activity, the ability to work at higher temperatures, lower cost, higher sulphur tolerance (<0.2 ppm), although they have lower FTS activity compared to cobalt catalysts.[10] The forward and reverse water gas shift (RWGS) reaction can handle hydrogen deficient feed by balancing the syngas ratio.[11] Thus, the properties of iron catalysts towards WGS are also critically important in determining the performance of Fe based catalysts for BTL applications. Low temperature Fe-based catalysts are reported to convert CO_2 effectively into high molecular weight hydrocarbons. This is attributed to their intrinsic RWGS activity, which is the first step involved in the CO_2 conversion to hydrocarbons.[11–13] Whereas the active FTS phase (CO hydrogenation) is believed to be the carbide phases, the WGS-RWGS sites are believed to be oxides species.[14,15] Iron carbide formation is important in order to obtain maximum activity towards FTS. The formation of carbide is achieved by treating the catalyst precursor with H_2, CO or with syngas.[16–21] Several carbide species have been detected such as ε-Fe_2C, ε'-$Fe_{2.2}C$, Fe_7C_3, χ-Fe_5C_2, and θ-Fe_3C,[22] with χ-Fe_5C_2 and θ-Fe_3C being the most stable of common species during FTS.[14,16,23–26] Highest CO conversion rates and hydrocarbon productivity have been associated with χ-Fe_5C_2, known as Hägg carbide.[13,27,28] The formation of Hägg carbide is affected by the gas composition and temperature. Using H_2 pre-treatment, metallic iron is mainly formed, which is susceptible to sintering and subsequently lower degree of carburization.[21,25,20] Both syngas and CO pre-treatment can transform the iron oxide precursor into χ-Fe_5C_2 at ~ 250°C and subsequently to θ-Fe_3C (cementite) at temperatures above 350°C.[14,26] Cementite has low FTS activity because it is associated with inactive carbon deposition.[14,23,29] Therefore, activation using pure CO at low temperatures is preferred.[26] χ-Fe_5C_2 carbide is also susceptible to oxidation, carbon deposition and attrition, especially in unsupported catalysts.[14,27,28,30] This could explain their higher initial activity but higher deactivation rate compared to supported iron catalysts.[21]

Supported iron catalysts show better catalytic stability[31] due to improved resistance towards attrition and sintering especially SiO_2 and Al_2O_3 as supports.[16,26,30–34] Wan et al.[33] reported that SiO_2 suppresses H_2 adsorption, facilitates CO adsorption, iron carburization and selectivity to heavier hydrocarbons, leading to more active catalysts compared to Al_2O_3,[35] although the run stability of Fe/Al_2O_3 catalysts is generally better than Fe/SiO_2 analogues. de Smit et al.[16] have reported strong interaction between Fe^{2+} ($Fe_{1-x}O$) species and the SiO_2 support, leading to formation of iron (II) silicate (Fe_2SiO_4) species. In addition, it may have interactions with promoters such as copper.[36] In the case of alumina, the formation of $FeAlO_3$ and $FeAl_2O_4$ species have also been reported.[35] Al^{3+} can easily replace iron cations and Fe can occupy vacancies in the defect alumina structure during activation and FTS.[22] Accordingly, the lower activity of supported Fe catalysts can be attributed to metal-support interactions affecting the reducibility and carburization. Al_2O_3 significantly improves the thermal and mechanical stability, preventing attrition and suppressing re-oxidation of the iron carbides.[31] It has been widely reported [11,13,16,22,23,26,30,36–40] that Cu can promote the reduction of hematite (Fe_2O_3) to magnetite (Fe_3O_4) suppressing sintering by lowering the reduction temperature. Shroff et al.[21] have suggested that Cu promotes the formation Fe_3O_4 and iron carbide nanoparticles and hence increasing the density of active sites. However, the effect of copper loading on iron carburization has not been studied in detail. The study of iron carbide during FTS is challenging due to the complexity and dynamic composition of the iron-based catalysts. Iron carbide clusters are usually pyrophoric and can be oxidised by air.[22]

The application of in situ X-ray methods have proved to be excellent tools for studying active phase formation and evolution during FTS.[41] The most commonly used methods for heterogeneous catalysts and material characterisation are X-ray absorption fine structure spectroscopy (XAFS) and X-ray diffraction (XRD).[42–45] XAFS is divided in two spectral regions, the X-ray absorption near edge structure (XANES) and extended X-ray absorption fine structure (EXAFS) that provide detailed information about the oxidation state and coordination environment of the absorber atoms.[16] Some authors[28,46] have used XANES measurements at pseudo in situ conditions, although exposure to air during sample handling may change the catalyst metal-phases composition. Carbide species on working iron-based FTS catalysts have been characterised by in situ XAFS-XRD at 1 bar,[16,47] and 10 bar[14] of pressure. However, to our knowledge, Fe-based catalysts have not yet been characterised in situ at pressures above 10 bar and hence closer to industrial FTS conditions (typically $\sim$ 20-45 bar[10]).

In the current work, a combined in-situ XRD/XAFS/mass spectroscopy (MS) set-up was used in order to reveal the iron-phases changes occurring over iron-based copper-promoted alumina catalysts during FTS at 18-20 bar. In particular, by studying the effect of copper loading on iron carbide phase formation and catalytic performance at different reaction temperatures without prior gas pre-treatment of oxide precursors. The catalytic performance of the catalysts was also evaluated in a fixed-bed reactor set-up to determine the catalytic behaviour after 100 h for FTS and water gas shift (WGS). Furthermore, in-situ FT-IR studies have been shown to be useful for understanding the nature of surface species formed and accumulating on the catalyst surface during reaction. FT-IR has been successfully used to prove that formate species are not key intermediates in the synthesis of methanol on copper catalysts where formate species remain adsorbed on the copper surface.[48,49] During WGS over Au-based catalyst,[50] these species are also present as spectators. In situ DRIFTS (diffuse reflectance infrared Fourier transform spectroscopy) investigations have verified the spectator role of formate species in WGS over Au-based and Pt-based catalysts.[51,52] Recently Parades-Nunez and co-workers[53] used in situ DRIFTS to report the presence of formate and carboxylate species resistant towards hydrogenation, they reported strongly adsorbed carboxylate species on Co-based alumina supported catalysts during FTS. Hence, in situ DRIFTS experiments have been carried out also in this work to study the effect of Cu loading on the formation, nature and accumulation of surface carbon-containing species during FTS.

Experimental Section

Catalyst preparation

Four alumina-supported iron-based catalysts with different copper loadings were prepared by incipient wetness impregnation. Fe loading was kept constant at 15 wt% for all catalysts. Cu loading was set to 0, 0.6, 2.0, and 5.0 wt%. The following notation was given for the catalysts: 15, 15/0.6, 15/2 and 15/5 i.e 15%Fe/Al2O3, 15%Fe0.6%Cu/Al2O3, 15%Fe2%Cu/Al2O3 and 15%Fe5%Cu/Al2O3 respectively. Fe(NO3)3.9H2O (Sigma-Aldrich, 98%) and Cu(NO3)2.3H2O (Acros Organics, 99%) were dissolved in deionised water, and added drop wise to the alumina support (ɣ-Al2O3 PURALOX SCCa series). The solution was dried overnight at 120°C, and then calcined in synthetic air at 300°C for 16 h. The calcination conditions were adapted from Rachmady and Vannice.[54]

Fischer-Tropsch synthesis

The catalysts were tested toward the Fischer-Tropsch synthesis in four parallel fixed-bed reactors (stainless steel, 10 mm inner diameter). The samples were diluted 1:6 with inert silicon carbide particles, in order to improve the temperature distribution along the catalyst bed. The samples were pre-treated with syngas (H2:CO = 2:1) at low temperature (20°Cmin-1 to 230°C for 24 h) in order to transform the iron oxide precursor into χ-Fe5C2. The experimental set-up and procedures is described in detail elsewhere.[55,56] After syngas pre-treatment, the samples were pressurised under He at 50 mLh-1 ramping 20°Ch-1 to 100°C. Then, 50 mLh-1 of syngas (H2:CO 2:1) was introduced using a ramp rate of 20°Ch-1 until 230°C. FTS was carried out at 20 bar at three different temperatures 230°C, 250°C and 270°C using a gas hourly space velocity (GHSV) of 1000 LKgcata-1h-1. Each temperature was keep for 100 hours and then changed using the same ramp rate. Low temperature conditions were tested with the aim to decrease CH4 production increasing C5+ yield since it is known that CH4 production is favoured at higher temperatures.[3] The analysis was limited to gas phase products (C1-C4), since liquid products were collected in a condenser trap before the GC.

Carboxylate species references by DRIFTS

Carboxylate species coming from acetic acid (Prolabo, 100%) and propionic acid (Sigma-Aldrich, 99.5%) were impregnated on ɣ-Al2O3 and commercial powder samples of Fe2O3 (Sigma-Aldrich, 99% < 5 microns), Fe3O4 (Sigma-Aldrich, 97 % 50-100nm) and FeO (Sigma-Aldrich, 99.9% <10 microns). Approximately 1.5 g of the powder samples were pre-dried at 120°C for 15 min, then impregnated with 5 ml of an aqueous acetic: propionic acid solution (1:1). The resulting suspension was stirred for ~ 1 h at room temperature. Finally, the samples were dried in an oven for 15 min at 120°C to release the remaining water. The resulting dried samples were characterised by DRIFTS as references to detect potential carboxylate species adsorbed on the surface.

Characterisation of fresh catalysts

The elemental composition (Cu/Fe wt% ratio) of the prepared catalysts was carried by X-ray fluorescence (XRF) analysis using a Rigaku Supermini200 equipment with a X-ray tube of 50 kV, 200 W Pd-anode. Fe dispersion on alumina was determined by CO chemisorption in a Micromeritics ASAP 2020 instrument. The samples (~100 mg) were loaded into a u-shaped quartz reactor enclosed by quartz wool plugs. The samples were first evacuated in He at 35°C for 60 min with subsequent H2 pre-treatment at 450°C for 5 h, using a ramp rate of 2°Cmin−1. After pre-treatment, the samples were evacuated in He at 450°C and 50°C for 60 min and 90 min, respectively. The adsorption isotherms were measured at 30°C in the CO partial pressure interval 0.05-450 mmHg. The adsorption isotherm was extrapolated to zero pressure to determine the volume of CO adsorbed by metallic iron atoms. The iron dispersion and average iron nanoparticle diameter were calculated using a similar approach to Rachmady and Vannice. [54]

The BET surface area, pore volume and pore diameter of the fresh catalyst samples were determined by N2 physisorption. The measurements were performed in a Micromeritics TriStar II 3020. The catalyst samples (~100 mg) were degassed overnight at 200°C prior to the analysis to remove any moisture from the sample. The reduction profiles of the calcined catalysts were studied by temperature-programmed reduction (TPR) in hydrogen (7 vol.%) diluted by nitrogen 50 mLmin-1. The analysis was carried out in a QUANTACHROME - ChemBET 3000. The samples (~100 mg) were loaded

into a U-shaped quartz reactor enclosed with quartz wool. The temperature was increased from room temperature to 800°C with a ramp rate of 10°C.min-1. The XRD patterns of the fresh samples were obtained by using a Bruker D8 Advance DaVinci instrument with a Cu anode (λ=1.54 Å). The diffractograms were collected for 120 min in the range 2θ=10-75°. The phase identification and the crystallite size of the catalysts were acquired in the evaluation software Diffrac.eva. Transmission electron microcopy (TEM) experiments were performed with a JEOL 2010F equipped with a field emission gun, operating at 200 kV accelerating voltage. The crushed catalysts powders were dispersed on a carbon supported Au mesh grid for TEM measurements. Element mapping in the catalysts before and after reaction was obtained by measurements in scanning (S)TEM mode coupled with an energy-dispersive X-ray spectroscopy (EDX) detector from Oxford instruments. Carbon, iron and copper maps in the catalyst were obtained by acquiring series of spectra when scanning the EDX probe that collect the X ray signal coming from specific atoms excitations due to the electron beam at the surface of a region of interest. At each pixel of the scan (0.5 nm x 0.5 nm) full EDX spectrum is acquired. The whole set of EDX spectra is then processed to obtain the chemical element map.

Combined in situ XANES/XRD/MS set-up

The in situ XANES/XRD/MS measurements were collected at the Swiss-Norwegian beam line (BM01B) at the European Synchrotron Radiation Facility (ESRF) in Grenoble, France. The iron phases and crystallinity evolution during FTS were monitored by in situ XANES and XRD as well as the CO conversion, CH_4 and CO_2 gas concentrations by an on-line MS. Figure 1 shows a scheme of the in situ experimental set-up.
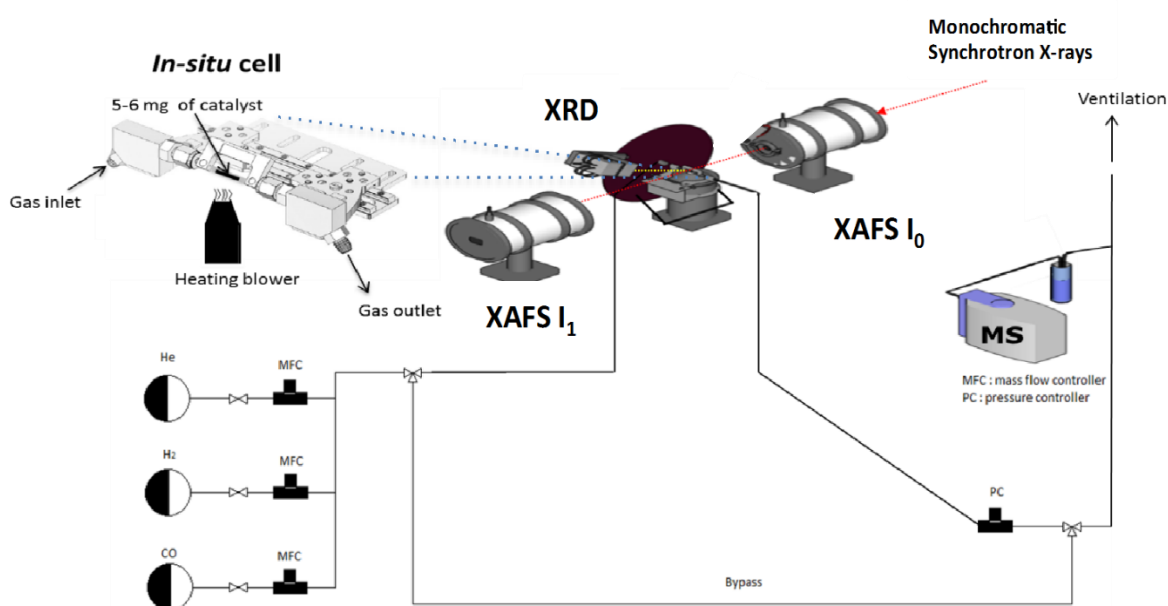

 Figure 1. Schematic drawing of the XANES/XRD/MS set-up. Adapted from ref. [59] Copyright (2012), with permission from Elsevier.

The experimental set-up has previously been validated for cobalt-based catalysts during FTS.[57–60] Around 5-6 mg of catalyst was placed inside a quartz capillary reactor (1.0 mm outer diameter) and set with glass wool (bed length ~ 1 cm). This type of capillary reactor has shown quasi plug flow reactor

performance.[61] The reactor was mounted in a stainless steel bracket and sealed with high temperature epoxy glue. Finally, the bracket was fixed to the in situ cell (left top side of Figure1), which has an inlet and an outlet for gases. A hot gas blower was used to provide heat. The operating conditions were the following: temperatures 230-250-280°C, pressure 18 bar, gas hourly space velocity (GHSV) ~ 15000 LKgcata-1h-1, syngas 64% vol. H_2, 32% vol. and 4% vol. A condenser trap was placed at the entrance of the MS to avoid condensed products entering and plugging the capillary coloumn. Ar was used as internal standard. Firstly, He was introduced to achieve the working pressure (18 bar) with the pressurization taking approximately 1 h. After ensuring no leaks, the temperature was increased from room temperature to 230°C using a ramp rate of 5°Cmin-1 under syngas (~ 4-6 h for each temperature step). The catalysts were exposed directly to syngas under FTS conditions. XRD and XANES data were alternately collected together with on-line MS data. A cycle of measurements took around 1 h, i.e. one X-ray diffractogram (25 min) and six XANES spectra (5 min). The ion chambers were optimised for iron K-edge energy (7112 eV) detection. Qualitative and quantitative analysis were carried out on the XANES part of the XAS spectra. Spectra of chemical standards (Fe0, FeO, Fe_2O_3, Fe_3O_4, and Fe_3C Fe_5C_2) representative of the possible chemical species in the sample were also measured. Linear combination fitting (LCF) was performed with the purpose of determining the evolution of iron phases during FTS using the Athena software.[62] Normalized XANES spectra for each dataset were reconstructed and fitted with linear combination of normalized XANES spectra of reference compounds. Each spectrum obtained by LCF was presented as a fractional composition of chemical standards.

In situ DRIFTS/MS set-up

DRIFTS experiments were performed in a Praying MantisTM high-temperature DRIFTS reaction cell from Harrick Scientific Corporation with ZnSe windows. A description of the reaction cell and the experimental set-up is presented in Figure 2. The spectrophotometer employed was a Nicolet iS50 FTIR spectrometer from ThermoFischer Scientific. DRIFTS spectra were recorded at a resolution of 4 cm−1 and 32 scans accumulation. DRIFTS spectra were reported as log (1/R) vs. wavenumber, where R is the sample reflectance. The analysis was performed in the aliphatic hydrocarbons and oxygenates regions with the aim of study the population and accumulation of carbon species on catalyst surface at ~ 1 bar pressure.
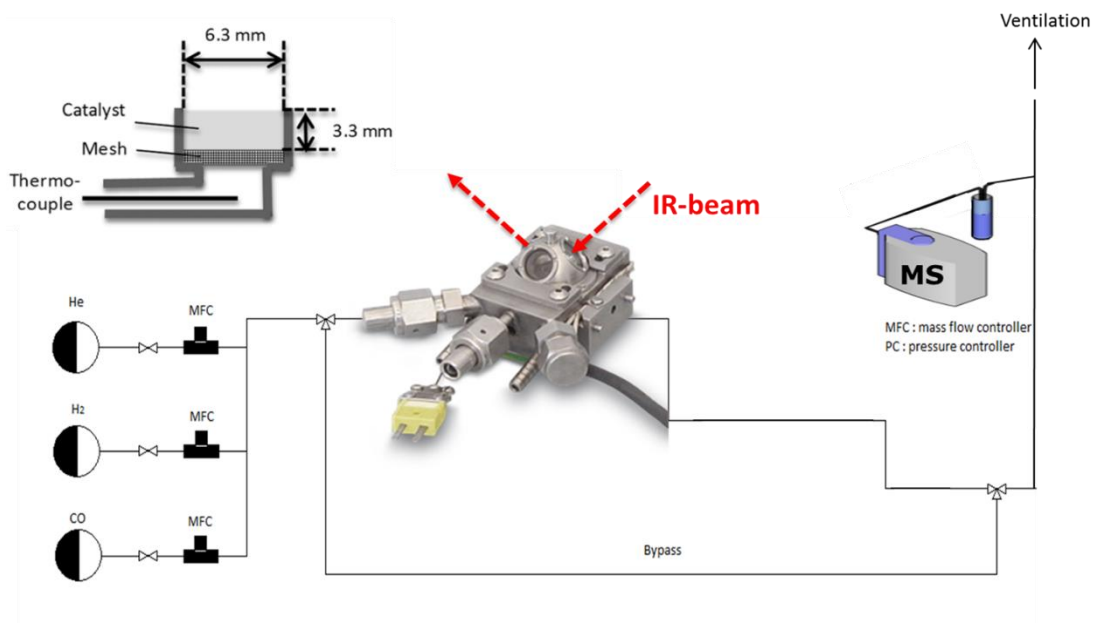
Figure 2. Schematic representation of the combined DRIFTS/MS set-up. Adapted from ref.[63] copyright (2015) Royal Society of Chemistry and ref.[64] copyright (2013) PCCP Owner Societies.

The stainless-steel reaction crucible of the DRIFTS cell contained about 80 mg of sample. The samples diluted with KBr (3:1) showed the better signal to noise ratio. Syngas contribution was collected over pure KBr at different temperatures (230, 250 and 280°C) then, subtracted from the catalysts spectra. Initially, the fresh catalyst was heated until 230°C under He atmosphere before syngas was introduced ($\sim$ 1 mL H_2, 0.5 mL CO Spectra were collected for approximately 3 h for each temperature. The catalysts were exposed directly to syngas to study the formation and accumulation of carbon species on surface. The system was operated at atmospheric pressure (1 bar) and the GHSV was about 1200 L.Kgcata-1h-1. The first and the last spectrum were treated and plotted for each temperature. The reactor effluent was analysed using an on-line Pfeiffer ThermoStarTM mass spectrometer. The CO conversion, CH_4, CO_2 and C2-C6 gas concentrations were measured. Similarly, a condenser-trap was placed before the entrance of the MS to avoid condensed products plugging.

Results and Discussion

Characterisation of fresh catalysts

The BET surface areas, pore volumes, average pore diameters, Fe dispersion and average Fe metal nanoparticle diameters are shown in Table 1. The catalysts composition determined by XRF measurements is also shown in this table, confirming that the experimental Cu/Fe values were close to the nominal ones. The decrease of pore volume and average pore diameter values as the metal loading increased, indicates that Cu was successfully introduced into the catalyst porous framework.[36] Cano et al.[65] have observed similar pore blockage and BET area decrease in copper promoted catalysts. Slightly enhanced iron dispersion was observed as the copper content increased, suggesting that higher copper loading facilitates the iron reduction. In addition, the average iron particle diameter indicated formation of smaller nanoparticles with increasing Cu loading, particularly at higher Cu loading (sample 15/5) where the average particle diameter was approximately half of the particle diameter compared with the unpromoted sample.

Table 1. Textural properties, dispersion and compositions of catalysts.

Sample	15	15/0.6
BET surface area (m^2g^{-1})	175	173
Pore volume (cm^3g^{-1})	0.52	0.53
Average pore diameter (nm)	9.7	10.0
Fe^0 particle[a] diameter (nm)	96	91
Cu/Fe wt% nominal	-	0.04
Cu/Fe wt%[b] experimental	-	0.02

[a] Calculated from CO adsorption assuming stoichiometry CO/Fe =1:2
[b] Atomic ratios relative to Fe and Cu composition measured by XRF

The X-ray powder diffraction patterns of the calcined samples are displayed in Figure 3 (a). The presence of hematite (Fe2O3) as the major iron phase is evident from the characteristic diffraction peaks at 2Ө values of 24.4, 33.4, 35.9, 40.9, 49.7, 54.2, 57.7 and 64.2.[23] Diffraction peaks corresponding to γ-Al2O3 were also observed, but CuO were not detected in the bimetallic Fe-Cu samples. This is in good agreement with previously reported results.[13,36] It has been pointed out that CuO is well mixed with the Fe2O3 phase.[26] The temperature-programmed reduction profiles are presented in Figure 3 (b). The intensities were normalized and given in arbitrary units. The TPR profiles displayed two regions, the first region at lower temperatures showing a sharp intense signal and the second one, at higher temperatures showing a broader signal with lower intensity.
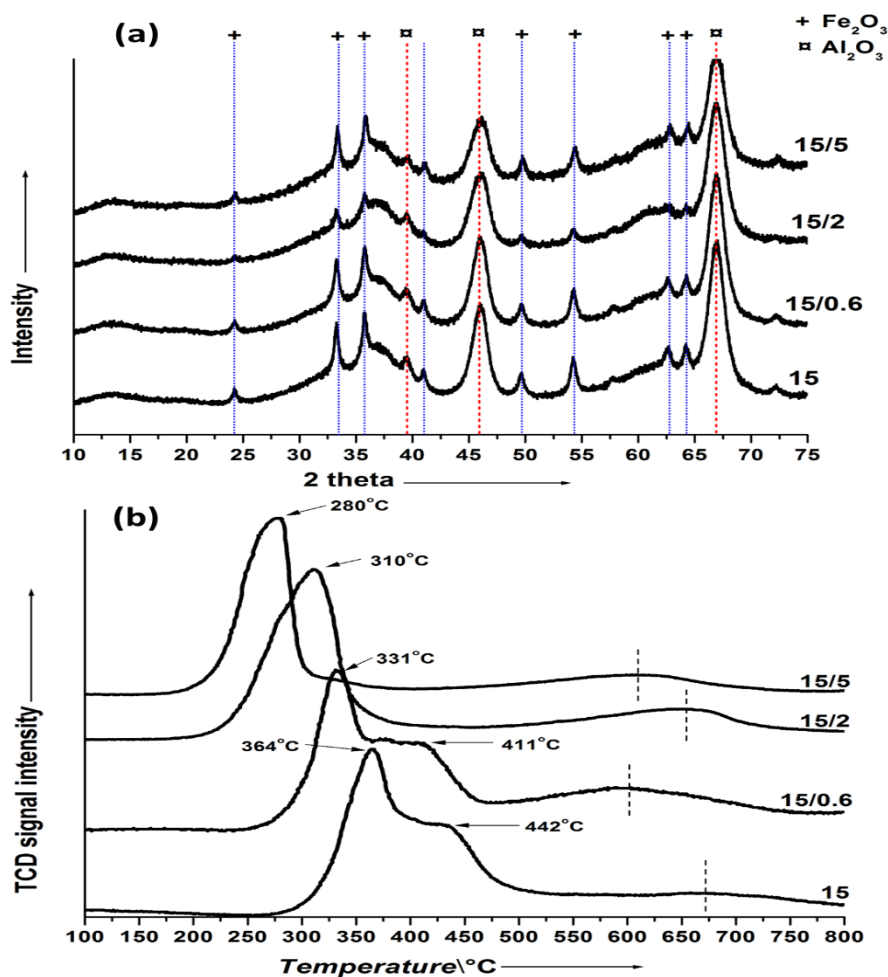
Figure 3. (a) XRD patterns and (b) TPR profiles of the freshly calcined catalysts.

The TPR profile of the Fe catalyst without Cu showed a peak at 364°C, and a plateau at 442°C after the curve levelled out at around 500°C. The first hydrogen consumption peak can be ascribed to the transformation of hematite to magnetite ($Fe2O3 \rightarrow Fe3O4$); while the plateau peak could be attributed to the reduction of Fe3O4 to FeO.[13] A similar profile was observed for the catalyst containing 0.6 wt% of Cu but the peaks were shifted to lower temperatures, indicating that also low Cu loading promotes the iron reduction. The TPR profiles of the 15/2 and 15/5 catalysts showed a narrow peak gradually shifted to lower temperature with increasing Cu loading. Clearly, there is an improvement in catalyst reducibility as the copper loading is increased. Distinguishing between the reduction of iron and copper oxides by TPR was not possible. This may suggest intimate contact between Cu and Fe particles since the combined reduction of $CuO \rightarrow Cu$ and $Fe2O3 \rightarrow Fe3O4$ has been reported.[32] It is well established that CuO reduction is carried out at lower temperatures than FexOy reduction. Metallic Cu crystallites start to nucleate early, providing dissociation sites for H2 and hence increasing the concentration of atomic hydrogen on the catalyst surface to assist in the reduction of Fe2O3 (spill-over).[16,26] The single reduction peak detected at lower temperatures for the 15/2 and 15/5 catalysts could be ascribed to the direct reduction of hematite to wustite ($Fe2O3 \rightarrow Fe3O4 \rightarrow FeO$) [66] promoted by the presence of higher Cu loadings. In addition, the slight H2 consumption detected between 600-700°C suggests the presence of species more difficult to reduce. The removal of oxygen at higher temperatures has been attributed to the reduction of iron oxide mixed compounds in strong interaction with the alumina support.[31–33] It is know that, Fe/Al2O3 catalysts undergo

iron phase transformations, i.e. $Fe_2O_3 \rightarrow Fe_3O_4 \rightarrow FeO \rightarrow Fe0$, but the reduction of FeO to metallic iron is hindered because the FeO phase (metastable phase of iron oxide below 570°C) can be stabilised on Al_2O_3,[66] which could further retard reduction to Fe0. According to these results, the reduction to Fe0 is still difficult due to the interaction of FeO with the alumina support, but the addition of Cu promotes the reduction of hematite to wustite.

Fischer-Tropsch synthesis in fixed-bed reactor

The CO conversion for each catalyst as a function of reaction temperature is shown in SI Figure 1. Addition of copper increased CO conversion at all temperatures. O'Brien and Davis[67] have previously observed a similar trend. Also Pendyala et al.[68] reported that CO conversion is found to increase with increasing copper loading for a series of iron copper promoted catalysts. The increased CO conversion with increasing Cu loading can be related to the hydrogen spillover effect on Cu that facilitates the reduction of iron oxide (TPR profiles Figure 3 (b)) and hence producing a large number of active sites.[16,26] The addition of 0.6 wt% Cu had a positive effect on the C5+ selectivity compared to the unpromoted sample, whereas for the CH4 and C2-C4 selectivities there was no significant effect (Figure 2 SI). There is a controversy in the literature about the effect of Cu on activity and selectivity.[65] Some authors have observed that Cu may have a positive effect on C5+ selectivity.[36,65,67] As expected, a rise in selectivity to light products and a decrease in C5+ selectivity were registered with increasing temperature due to a decrease in the chain growth probability.[69] For higher Cu loadings i.e. the 15/2 and 15/5 catalysts, the selectivities to CH4, and C2-C4 were relatively temperature independent, although a slight increase in C5+ selectivity for the 15/2 catalyst was observed (Figure 4).
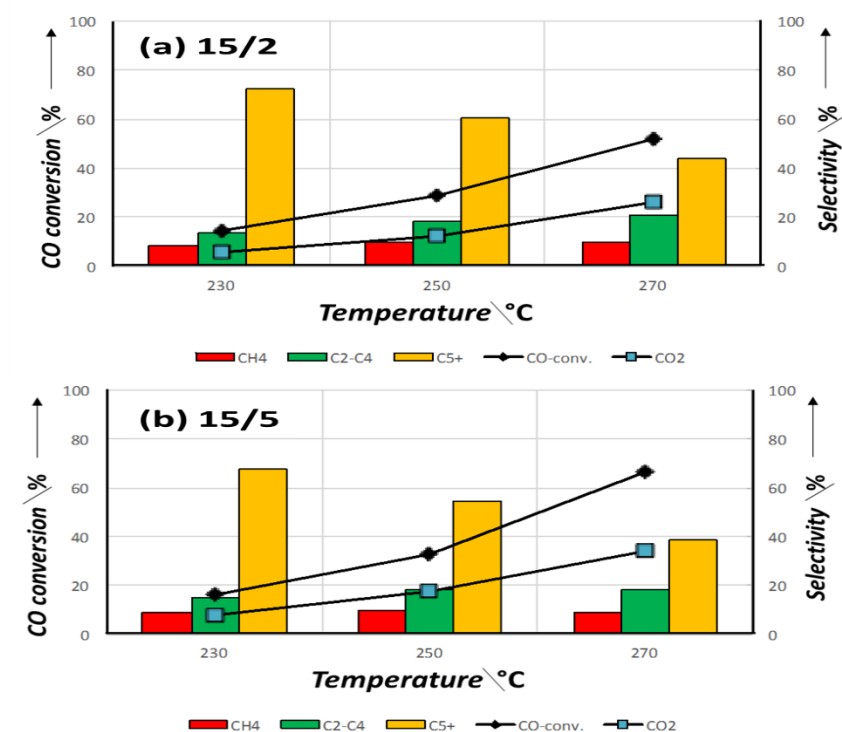

Figure. 4. CO conversion, hydrocarbon and CO2 selectivities and as a function of reaction temperature. H2/CO =2, 230-250-270°C, 20 bar, GHSV ~ 1000 LKgcata-1h-1 ~ after 100 h on stream at each temperature.

Figure 4 shows that the CO2 selectivity increased with CO conversion and temperature except for the unpromoted catalyst (Figure 2 SI). The CO2 selectivity can be considered as a measure of the water gas-shift (WGS) activity;[21] therefore the WGS activity of the unpromoted catalyst was high at lower temperatures (230-250°C) compared to the promoted catalysts. This trend was reverted at 270°C for the 15/2 and 15/5 catalysts where, the 15/5 catalyst showed the highest WGS activity at 270°C. The 15/0.6 catalyst showed the lowest CO2 selectivity in the entire temperature range. In summary, low Cu loading (15/0.6 catalyst) enhanced C5+ selectivity while high Cu loading (15/2 and 15/5 catalysts) increased CO conversion and WGS activity under the conditions studied. Figure 3 SI shows the olefin to paraffin ratios (O/P) for light hydrocarbons (C2-C6) vs. temperature. C3 hydrocarbons showed the maximum O/P while C2 hydrocarbons showed the minimum O/P for all temperatures. De la Peña et al.[70] reported a similar tendency in agreement with our results. Ethene is 10-40 times more reactive than the other olefins and is mainly hydrogenated to ethane.[71] This could explain the low O/P ratio detected for C2 hydrocarbons. Additionally, ethene could be involved in the chain growth process.[72] The decrease in O/P ratio with carbon number is caused by intraparticles diffusion effects of molecular weight hydrocarbons.[73] Higher molecular weight α-olefins have longer residence time within the catalyst pores, thus increasing the possibility of secondary reactions.[70-75] It has been reported [76,77] that an increase in O/P ratio could be related to higher degree of carbon deposition, because α-olefins may be transformed into more complex carbon species that can be accumulated on the catalyst surface. The addition of 0.6 wt% of Cu did not affect the O/P ratio compared to the unpromoted catalyst. However at higher copper loading (15/2 and 15/5 catalysts) a significant decrease in the O/P ratio was detected throughout the entire temperature range. This result can be explained by the high hydrogenation activity of metallic copper,[11] thus more reactive hydrogen is present on the catalyst surface to hydrogenate the primary α-olefins. As expected, the O/P ratio decreased with increasing reaction temperature.[71] Our findings corroborate that Cu promotion can increase CO conversion, decrease the O/P ratio and hence enhance the yield of saturated hydrocarbons and also increase WGS activity.[78]

In situ XRD/XANES/MS characterisation at FTS conditions

The in situ XRD patterns of 15/2 and 15/5 catalysts during FTS are shown in Figure 5. The samples were directly exposed to syngas in order to study the effect of Cu addition on the formation of different crystalline iron phases.
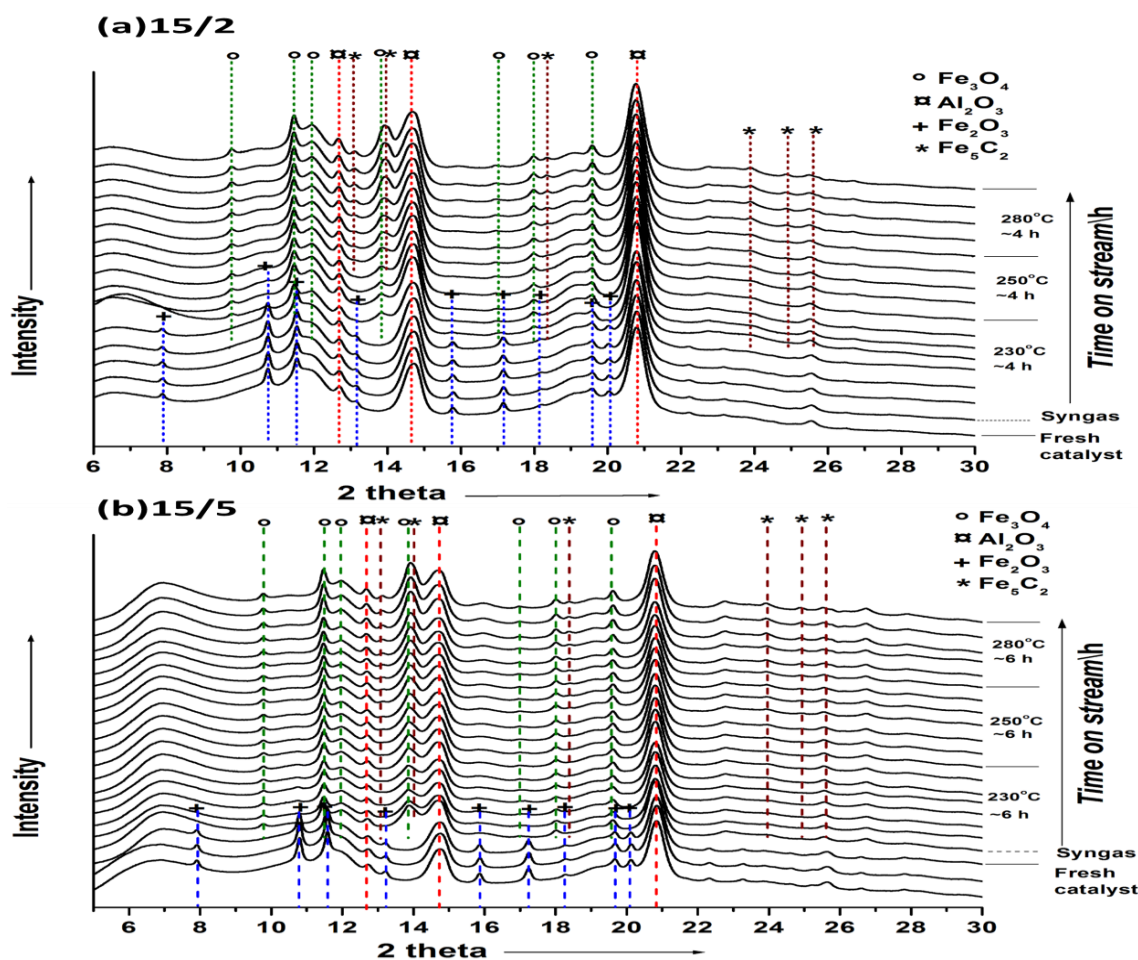
Figure 5. In situ XRD evolution during FTS at 18 bar, H2/CO =2, 230-250-280°C and GHSV ~ 15000 LKgcata-1h-1 ~14-18 h on stream: (a) 15/2 and (d) 15/5 catalysts.

The in situ XRD data also confirmed Fe2O3 as the predominant iron phase for the fresh catalysts. After reaching 230°C in syngas, the initial Fe2O3 was converted into Fe3O4. For 15/2 and 15/5 catalysts Bragg reflections at 2θ values 12.8°, 13.9°, 18.2°, 24° and 25° started to appear, corresponding to formation of Hägg carbide (χ-Fe5C2) crystallites. It has been reported that Fe3O4 transforms into carbide in the presence of Cu during FTS.[21,26] The diffracted signals became more pronounced at 250-280°C although the main peak diffraction of Fe3O4 ~ 2θ = 13.7 overlapped with the main peak reported for Hägg carbide at 2θ = 13.9.[14,16] Such overlap between Hägg carbide and magnetite has been previously reported.[21] For that reason, accurate evolution of Hägg carbide nanoparticle diameter using peak broadening was not possible. The iron nanoparticle diameters estimated from CO adsorption dispersion measurements (Table 1) suggested smaller nanoparticles for 15/2 and 15/5 catalysts. de Smit et al.[22] stated that Hägg carbide is formed on iron-based catalysts as small nanoparticles giving broadened Bragg reflections with low intensity, which is in line with the weak diffraction signals observed here. Smaller and well-dispersed iron nanoparticles carburize faster and they are more resistant towards oxidation than larger particles.[17,79] In the case of the 15 and 15/0.6 catalysts (Figure 4 SI), Bragg reflections corresponding to Hägg carbide phases were not detected even at higher temperatures, suggesting that Fe-Al2O3 interactions inhibited further iron carburization. A Cu loading of 0.6 wt% is not sufficient to promote the iron carburization. In summary, in situ XRD measurements suggested the presence of Fe5C2 and Fe3O4 crystalline phases for the catalysts promoted with 2 and 5 wt% of Cu. The CO conversions, as well as CO2 and CH4 concentrations were

also measured in order to monitor the catalytic performance. Table 2 displays these measurements at the end of each isothermal step.

Table 2. FTS catalytic performance during in situ XRD measurements in the capillary reactor at 18 bar, H2/CO =2, 230-250-280°C and GHSV ~ 15000 LKgcata-1h-1. Note that CO2 and CH4 are gas phase concentrations (%) and not selectivities, since MS analysis does not allow for full product analysis of heavier components. MS data is shown in Figure 5 SI.

Sample	15			15/0.6			15/2			15/5		
Temp. (C)	230	250	280	230	250	280	230	250	280	230	250	280
CO conv. (%)	0.05	0.2	1.2	1	2	10	5	15	51	1	11	42
CO$_2$ conc. (%)	0.3	0.3	0.4	0.2	0.3	1.3	0.7	1.7	12.5	0.6	1.3	7.4
CH$_4$ conc. (%)	0.01	0.04	0.2	0.02	0.1	0.7	0.3	0.7	2.6	0.2	0.8	3.3

The unpromoted catalyst showed lower CO conversion even with increasing temperature, suggesting that the catalyst was hardly active for FTS. A similar trend was observed for the 15/0.6 catalyst, although a slight improvement in catalyst performance was detected at 280°C. The 15/2 and 15/5 catalysts exhibited a gradual increase in CO conversion with increasing temperature as well as increasing CH4 and CO2 concentrations (Table 2 and Figure 5 SI). The presence of XRD signals corresponding to Hägg carbide (Figure 5) could be associated with the improvement in CO conversion for those catalysts. Moreover, the CO2 concentrations were considerably higher at 280°C suggesting significant WGS activity. It is established that for Fe-based catalyst during FTS, the extent of WGS activity is limited by the amount of product water available. Therefore a large fraction of the water formed is consumed by the WGS reaction and most of the oxygen from the reacting CO is rejected as CO2.[12,21] In agreement with the fixed-bed reactor experiments (section 3.2), 15/2 and 15/5 catalysts were more active towards WGS especially at higher temperatures. It is important to note that for the in situ FTS experiments; the space velocity was higher than in the FTS experiments in section 3.2, it is known that lower space velocity leads to enhanced CO conversion due to longer residence time of reactants in catalyst active sites.[3] The samples were not diluted, which may also affect the activity and selectivity data.[80]

The evolution of iron phases was followed by fitting the in situ XANES data collected during FTS with the spectra of iron standards (FeO, Fe2O3, Fe3O4, Fe3C and Fe5C2) using linear combination fitting (LCF) provided by the Athena software.[62] XANES data fitting has been previously used successfully on iron-based catalysts to determine the concentrations of different iron phases during FTS conditions.[14,16,28,46,47] Figure 6 displays an example of a complete XANES data set evolving during FTS (a) and a typical fit of a XANES spectrum using the iron standards (b). The best fitting was obtained including Fe2O3, Fe3O4 and Fe5C2 standards. Fe3C was not relevant for the fit even at 280°C. Higher temperature is need to form Fe3C carbide.[14]
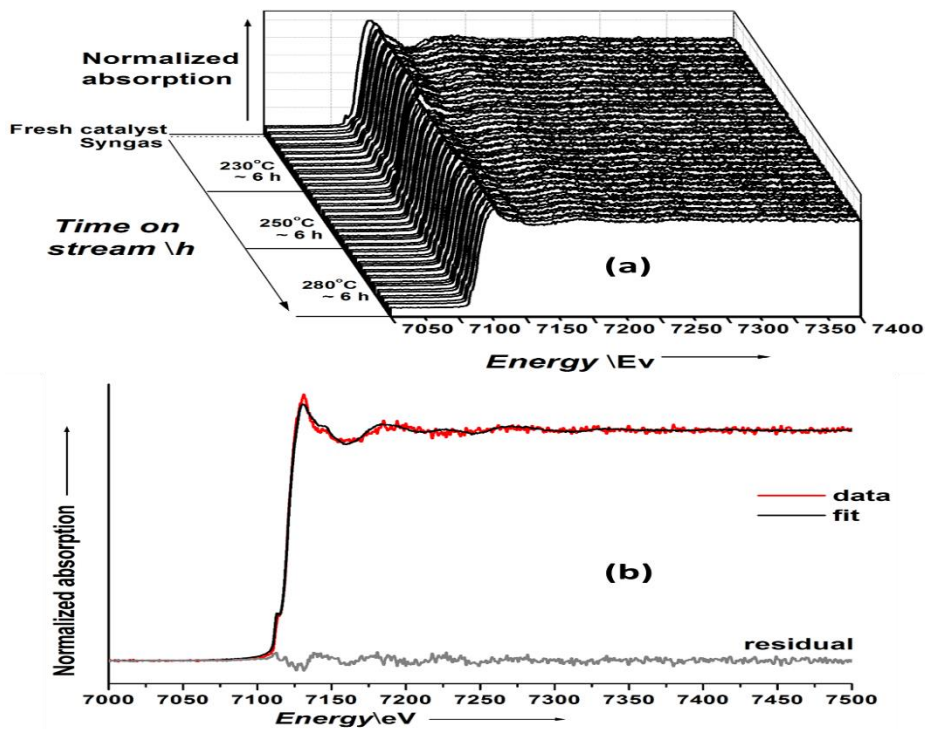
Figure 6. XANES data of the 15/5 catalyst at 18 bar, H2/CO =2, 230-250-280°C and GHSV ~ 15000 LKgcata-1h-1: (a) data evolution at different temperatures, (b) experimental XANES spectrum with the linear combination fitting and residual.

At room temperature in He atmosphere, XANES spectra of fresh catalysts showed a pre-edge at ~7113.5 eV corresponding to the 1s → 3d electronic transition and a white line edge attributed to the transition 1s → 4p at ~7123 eV, both characteristic for Fe2O3.[81] and in agreement with the in situ XRD results. After syngas introduction and pressurization to 18 bar, XANES spectra of the catalysts did not show abrupt changes in absorption intensity or significant energy shifts even at higher temperatures. Minor changes in absorption pre-edge intensities and a slight shift towards lower edge energies with increasing temperature and time on stream were detected, suggesting a slow progressive reduction of the catalyst samples.[47] Figure 7 displays the evolution of the iron phases at the three different temperatures followed by XANES linear combination fitting for 15/2 and 15/5 catalysts.
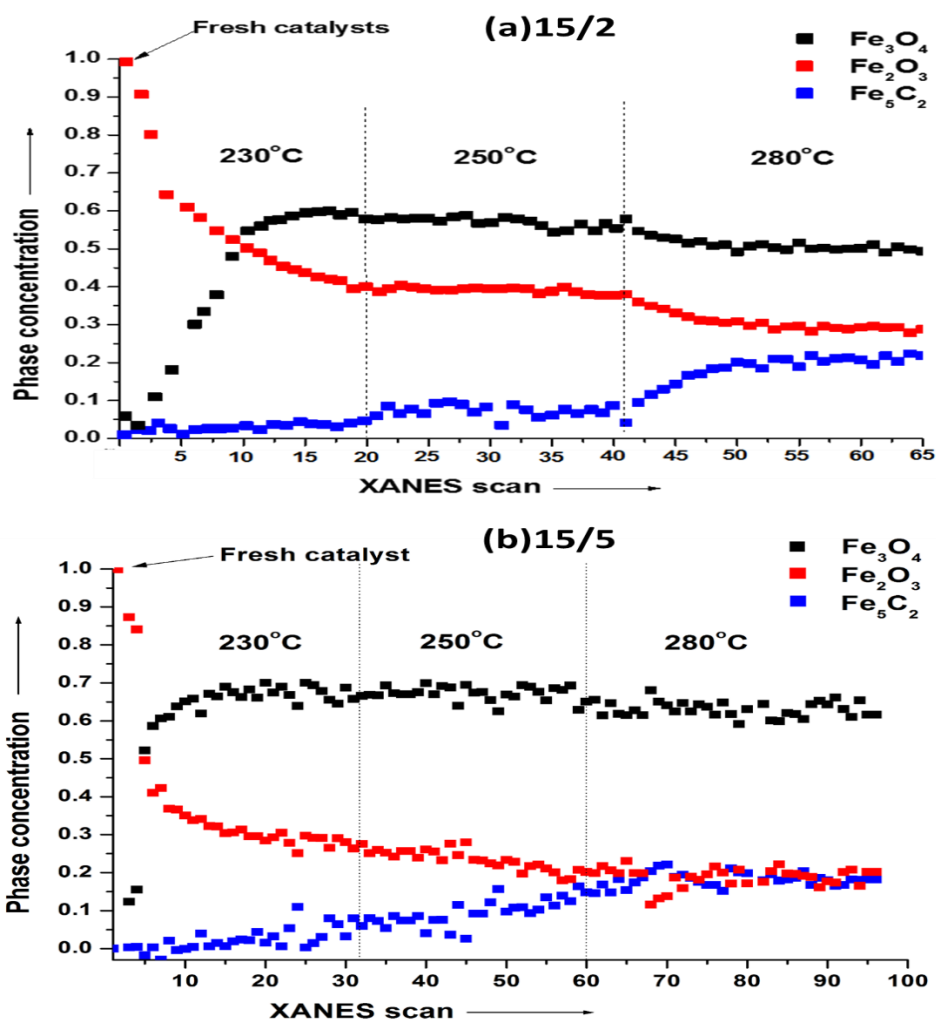
Figure 7. In situ XANES iron phase concentration profiles at 18 bar, H2/CO =2, 230-250-280°C and GHSV ~ 15000 LKgcata-1h-1 ~ 14-18 h on stream: (a) 15/2 and (b) 15/5 catalysts.

Initially, the fresh catalysts showed a progressive reduction of hematite (Fe2O3) to mainly magnetite (Fe3O4) and formation of Hägg carbide (Fe5C2). Two reduction steps were observed; a rapid one at 230°C followed by a slow step at 250-280°C. Hägg carbide was not detected in the 15 and 15/0.6 catalysts even at 280°C according to the LCF (Figure 6 SI), which can be ascribed to the strong Fe-Al2O3 interaction[31–33] and subsequent lack of metallic Cu nucleation sites to promote iron carburization. However, when the catalyst was promoted with 2 and 5 wt% Cu, a gradual slow carburization occurred which became more pronounced at 250°C and 280°C. These results are in agreement with the in situ XRD results (Figure 5). The XANES results confirm that at FTS working conditions, Fe2O3 is transformed to Fe3O4 and then further reduced to Fe5C2 at a rate, which is depending the copper loading. Table 3 summarizes the fraction of the iron phases detected for the 15/2 and 15/5 samples at the end of each isothermal step and their corresponding experimental errors.

Table 3. Iron phases concentration during FTS at 18 bar, H2/CO = 2, 230-250-280°C and GHSV ~ 15000 LKgcata-1h-1.

Sample	15/2			15/5		
Temp. (^{o}C)	230	250	280	230	250	280
(%) Fe_2O_3	39±2	38±2	28±3	26±2	20±2	18±3
(%) Fe_3O_4	58±2	56±2	50±2	67± 2	63±2	62±2
(%) Fe_5C_2	3±3	5±3	22±2	7±3	17±3	20±2

For the fresh 15/2 catalyst at 230°C, the initial Fe2O3 was converted into a mixture of about 58 % of Fe3O4, approximately 3 % Fe5C2 and 39% of remaining Fe2O3 (Table 3). Carbide formation was still slow at 250°C since only ∼ 5% Hägg carbide could be detected. At 280°C, the degree of carburization increased significantly reaching 22%. For the 15/5 catalyst, Hägg carbide content evolved slowly from 7% at 230°C to 17% at 250°C and finally to 20 % at 280°C. Increasing carburization degree at higher temperatures also resulted in higher catalytic activity as can be observed in Table 2. The 15/2 and 15/5 catalysts showed analogous CO conversion, CH4 and CO2 concentrations at 280°C after 14 and 18 h on stream respectively, reflecting the similar final Hägg carbide fraction in the two catalysts (20-22%). It seems to be a limit in the iron carburization (around 20-22%) at the present conditions even for higher copper loadings (5 %wt) and after 18 hours on stream, notwithstanding Cu nanoparticles could agglomerate parallel with Cu loading.[82] Note that iron carburization can also be influenced by H2 and CO partial pressures and the temperature of the system through the thermodynamic equilibrium between the different iron oxide and carbide phases.[83] Pendyala et al.[68] studied the effect of gas activation for varying Cu promoter levels in Fe-based catalyst for FTS. They found that CO conversion increased with increasing copper loading up to 2 % for syngas activated catalysts, and slightly decreased with further increase in copper (5 %) loading. They attributed this trend to a higher carburization degree measured in the sample with 2 % Cu loading. Apparently, 2 wt % Cu is more rapidly activated by syngas at 280°C than 5 wt% Cu (more Cu agglomerates), due to accelerating the spillover effect for iron reduction and then carburization (Figure 7) leading to a slight increase in CO conversion (Table 2) and CO2 production (Figure 5 SI).

Ex situ TEM characterisation: Fresh and used catalyst

The initial and final morphology of the fresh and used catalysts recuperated from the capillary reactor were characterised by TEM. Some micrographs at medium and high-magnification of the 15/5 fresh and used catalysts are shown in Figure 8.
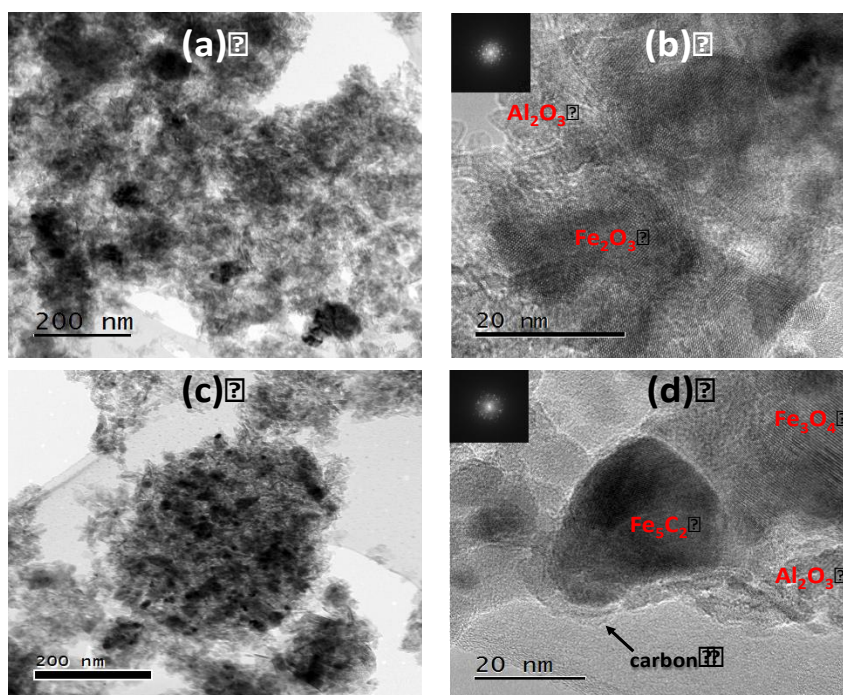
Figure 8. TEM images of the 15/5 catalyst (a, b) before FTS and (c, d) after FTS at 18 bar, H2/CO =2, 230-250-280°C and GHSV∼ 15000 LKgcata-1h-1 and 18 h on stream.

Figure 8 shows that the catalyst morphology changed after FTS. Before reaction, clusters of around 100 nm having irregular shape are observed (Figure 8 (a)) while after reaction, small spherical/elliptical nanoparticles in dark contrast of size 10-30 nm (Figure 8 (c)) are perceived. Figure 8 (b) displays a typical high resolution TEM image of the fresh catalyst, showing the presence of disordered clusters arising from stacking faults, a characteristic morphology of γ-Al2O3[84] and some regions corresponding to single α-Fe2O3[85] crystals, also confirmed by electron diffraction.[86] Figure 8 (d) displays a high-magnification image of the used catalyst where the initial α-Fe2O3 has been transformed into Fe3O4[87,88] and partially into small nanoparticles (20-30 nm) of Hägg carbide according to the d spacing and morphology,[21,26,89] also confirmed by electron diffraction.[90] The presence of disordered stacking clusters from γ-Al2O3 was also observed (Figure 8 (d)). These results are in good agreement with in-situ XRD/XAFS measurements, where the same iron oxide and carbide phase were detected. An amorphous carbon surface layer with 2-3 nm thickness was detected after FTS, probably corresponding to hydrocarbon-wax accumulated on the carbide particles and Al2O3 rather than on Fe3O4 (Figure 8 (d)), which is typically observed on iron catalysts after FTS or after activation in CO or syngas.[21,26,60] Amorphous carbon could cover parts of the iron carbide nanoparticles protecting them against air re-oxidation.

(a)

Cu

300nm   300nm   300nm

☐Fe ☐Al ☐O

(b)

Cu

300nm   300nm   300nm

☐Fe ☐Al ☐O
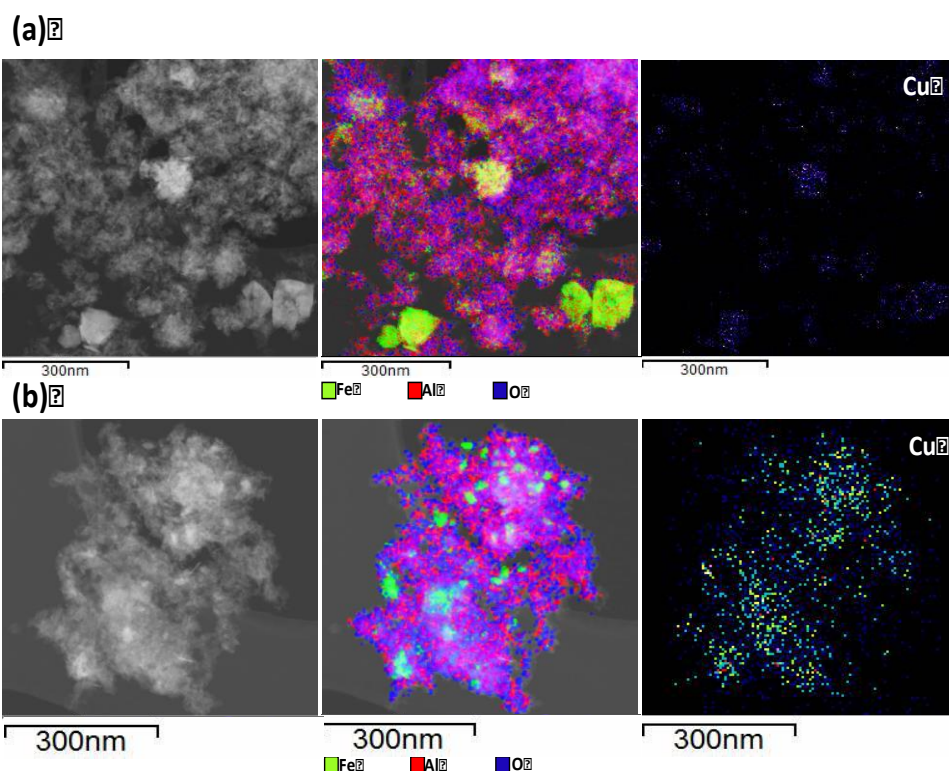
Figure 9. High-annular dark-field images STEM and elemental mapping EDX from the 15/5 catalyst (a) fresh calcined, (b) after FTS at 18 bar, H2/CO =2, 230-250-280°C and GHSV ∼ 15000 LKgcata-1h-1∼ 18 h.

STEM-EDX analyses were performed in order to map elemental compounds on catalyst surface[91] such as iron, oxygen, aluminium and copper distribution in the catalysts before and after reaction. Figure 9 (a) indicates that before reaction iron oxide particles of around 100 nm of diameter were dispersed and mixed with the alumina support. Elemental mapping suggested that Cu was well mixed with Fe. Mapping after FTS (Figure 9 (b)) shows the presence of small Fe nanoparticles in the range 10-30 nm confirming that Cu is still associated with Fe. TEM and STEM-EDX results confirmed that magnetite was transformed into iron carbide in the presence of syngas during FTS, causing magnetite crystallites to break up into smaller crystallites of iron carbide nanoparticles, demonstrating a decrease in the metal-support interaction. A schematic representation of these results is shown in Figure 10. The formation of carbide was promoted in the presence of copper (2-5 wt%), which has also been observed by Shroff et al.[21] and Yaming et al.[26]

Figure 10. Suggested mechanism of Fe-Cu/Al2O3 FTS catalysts for carbide formation.

In situ DRIFTS characterisation during FTS at atmospheric pressure

Copper can also promote formation of oxygenates since it favours the molecular adsorption of CO and CO2 with subsequent slow disso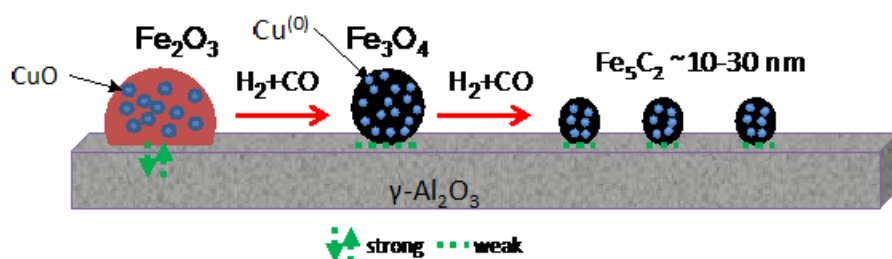ciation, leading to oxygen incorporation into the FTS hydrocarbon products.[39] However, due to the acidity of the alumina support some of these compounds may remain strongly adsorbed on the catalyst surface. Bianchi et al. [92] reported that surface carbonate species are irreversibly formed on copper-containing catalysts. Therefore, the presence of oxygenated species on the catalyst surface is expected. In situ diffuse reflectance infrared Fourier transform spectroscopy (DRIFTS) was employed for in situ studies of iron-based Fischer-Tropsch catalysts at relevant operating conditions. Figure 11 displays the in situ DRIFTS spectra collected during FTS for the 15/2 and 15/5 sample under 1 bar pressure. Once syngas was introduced, several bands related to oxygenated compounds were rapidly developing as well as weak bands related to aliphatic hydrocarbons.
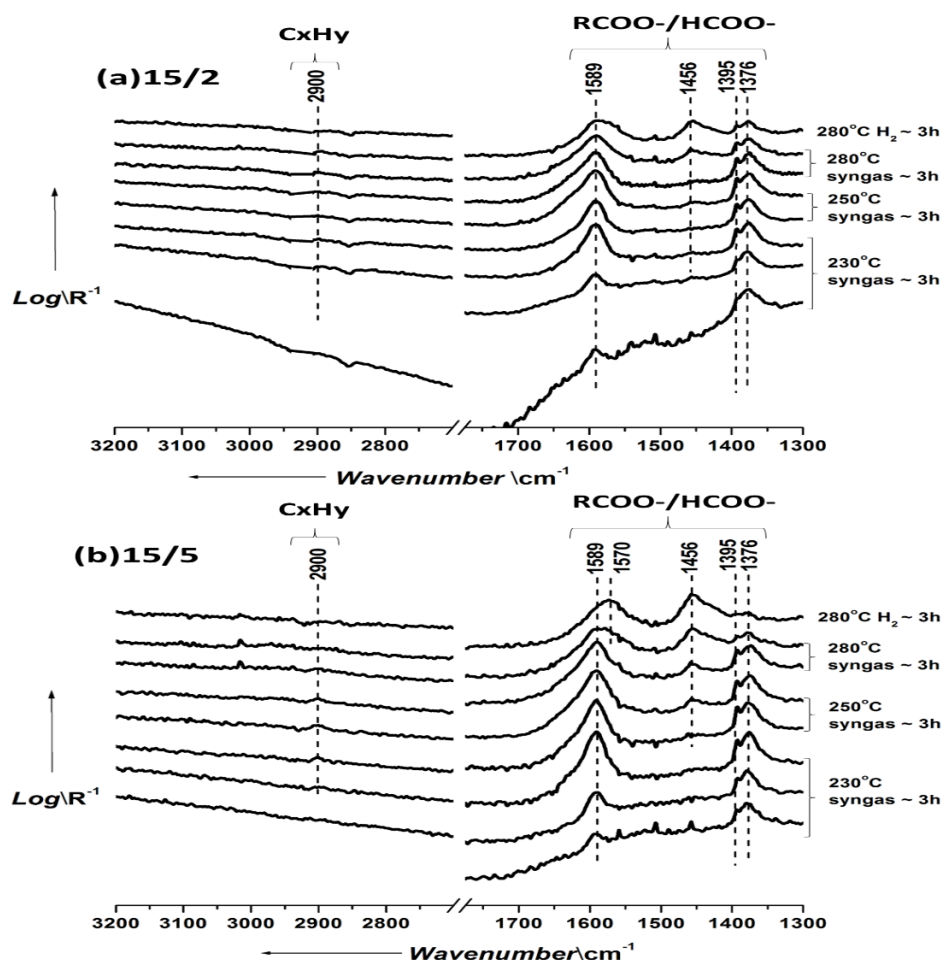
Figure 11. In situ DRIFTS spectra collected at various temperatures and time on stream over the prepared catalysts: (a)15/2 and (b)15/5. FTS at atmospheric pressure, H2/CO =2, 230-250-280°C and GHSV ~ 1200 LKgcata-1h-1.

Low-intensity bands associated with the stretching vibrations of methylene groups (-CH2-) at 2900 cm-1 [95] were detected in the 15/0.6, 15/2 and 15/5 catalysts (Figure 7 SI and Figure 11) indicating, poor presence of alkane chains (wax) on the catalyst surface at the applied conditions (atmospheric pressure, 1 bar). Three bands at 1589, 1395, 1376 cm-1 assigned to formate species adsorbed on the alumina surface[53] increased in intensity with temperature. An additional band at 1456 cm-1 also increased in intensity (associated with another band overlapped with the formate band at around

1589 cm−1 [93]). A significant increase in intensity of this band is observed for the 15/2 and 15/5 catalysts which is associated with carboxylate species adsorbed on alumina.[96] At 280°C the bands at 1395 cm-1 and 1376 cm-1 decreased in intensity. This bands correspond to the bending stretching mode of the C-H bond in formate species and to the asymmetric stretching mode of the O-C-O bond, respectively.[53] This can indicate a probably transformation of formate species to methanol[94] or to carboxylate species at higher temperatures. Recently, Lorito et al.[93] reported the presence of two types of formate species, "slow and fast formate" during FTS using in situ DRIFTS on Co-based alumina catalyst. They suggested that the "fast formates" could be intermediates in the formation of methanol while the "slow formates" remain adsorbed on the support. The surfaces of 15/2 and 15/5 catalysts were relatively clean from carboxylate species at 230-250°C, while for the 15/0.6 catalyst, carboxylate band (1456 cm-1) appeared already at the beginning of the reaction (Figure 6 SI). An explanation for this difference could be related to the H2 spillover at the Cu metal sites, enabling decomposition of carboxylate species at lower temperatures. Formation of carboxylate species is more pronounced at higher temperatures also at higher Cu loadings, since the carboxylate band at 1456 cm-1 was more intense at 280°C for the 15/5 catalyst. These results may indicate that higher Cu loading leads to accumulation of carboxylate species especially on the alumina surface. Similar carboxylate species adsorption on alumina has also been reported by others authors.[39,92]

 After feeding H2 diluted with He (10:1) at 280°C for the 15/2 and 15/5 catalysts the bands associated to formate species at 1395 cm-1 and 1376 cm-1 vanished while the band at 1589 cm-1 showed a slight shift to lower wavenumber (1570 cm-1) and the band at 1456 cm-1 corresponding to carboxylic species adsorbed on alumina increased in intensity. Paredes et al.[53] and Lorito et al.[93] have reported the presence of two types of formate species with different decomposition rates in H2, while the carboxylate species adsorbed on alumina remained unaffected on Co/Al2O3 FTS catalysts. Peña et al.[76] and Kistamurthy et al.[97] have observed the presence of resistant carboxylic acids strongly adsorbed on the alumina surface on used Co/Al2O3 FTS catalysts. Zhang et al.[40] reported the presence of carbonate species between 1572-1580 cm-1 on Fe-Cu-based catalyst exposed to air, while de Smit et al.[98] observed formation of carbonate species by in situ XPS during syngas treatment over iron-based FTS catalyst at atmospheric pressure (1 bar). They also reported that the carbonate species could hinder carbide formation and that they slowly desorb at higher temperatures to about 450°C.[40] Carbonate and carboxylate species are not readily separated, because both characteristic bands are situated between 1343 and 1410 cm−1.[99] In summary, 15/2 and 15/5 catalysts maintained a surface clean from carboxylic species at 230-250°C, but at higher conversions (280°C) the carboxylic species may migrate to and accumulate on the alumina support. From Table 4 can be observed that, CO2 concentrations were higher than CH4 and C2-C6 concentrations confirming significant WGS activity for the 15/2 and 15/5 catalysts. Our results suggest that oxygenated compounds such as formate carboxylate are important carbon species on working iron-based catalyst surface to be consider for studying reaction mechanisms and deactivation investigations during FTS.

Table 4. FTS catalytic performance during DRIFTS at atmospheric pressure, H2/CO =2, 230-250-280°C and GHSV~ 1200 LKgcata-1h-1. Note that CO2 and CH4 are gas phase concentrations (%) and not selectivities, since MS analysis does not allow for full product analysis of heavier components.

Sample	15	15/0.6		15/2			15/5		
Temp. (C)	280	250	280	230	250	280	230	250	280
CO conv. (%)	0.6	0.4	2	2	3	6	1	2	5
CO2 conc. (%)	0.16	0.08	0.26	0.12	0.27	0.51	0.14	0.24	1.03

CH₄ conc. (%)	0.10	0.04	0.14	0.07	0.16	0.32	0.07	0.16	0.57
C₂-C₆ conc. (%)	0.14	0.12	0.18	0.12	0.17	0.30	0.11	0.18	0.38

Several carboxylate references were prepared and characerised using the same DRIFTS conditions, in order to compare the bands at similar wavenumber of these references with bands obtained on the working catalysts to identify the carboxylate species accumulated on the catalyst. The comparison between the spectrum of the 15/5 catalyst and the spectra of synthetized carboxylate references is shown in Figure 12.
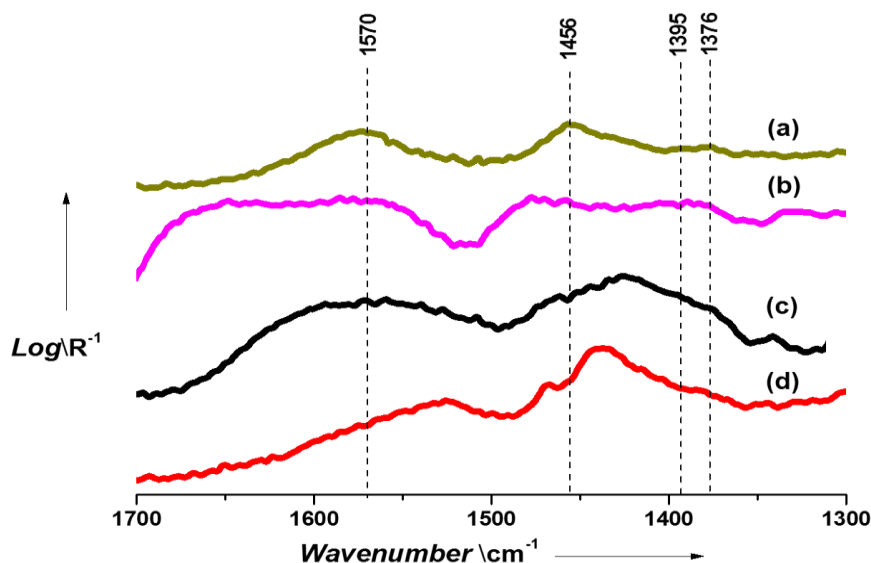

Figure 12. DRIFTS spectra comparison after exposure to hydrogen at 280°C (H2: He 10:1) during ~ 1 h: (a) 15/5 catalyst after FTS (atmospheric pressure, H2/CO =2, 230-250-280°C and syngas~ 1200 L.Kgcata-1.h-1), carboxylate references synthetized using acetic acid and propionic acid solution impregnated over commercial: (b) γ-Al2O3, (c) FeO and (d) Fe2O3.

The bands related to carboxylic species were not observed on Fe3O4, even before the hydrogenation step (plot not included), suggesting that the surface of this commercial sample were not susceptible for deposition of carboxylate species or to form complexes, although formation of carboxylate acidic group complexes with Fe3O4 nanoparticles[100–102] has been reported. The reference impregnated on FeO and Fe2O3 showed weak IR bands at frequencies comparable to the 15/5 catalyst. It has been reported that the iron cations Fe2+ and Fe3+ can separately form complexes with carboxylate ligand groups.[103] The IR spectrum of the γ-Al2O3 treated with carboxylic acid exhibited peaks of similar wavenumbers as detected in the 15/5 sample i.e. ~ 1570 and 1456 cm-1. According to the carboxylate references, the catalyst surface was covered by carboxylic species adsorbed on the alumina surface and Fe2O3/FeO sites. These observations support the hypothesis that once the carboxylate species are formed on active sites, they can migrate to the alumina and remain strongly adsorbed, although they may also form bonds with Fe2+ or Fe3+ in iron oxides (FexOy). Such complexes are probably obstructing further iron carburization, and directly affecting the FTS active site formation. The suggested mechanism is illustrated in Figure 13. Accumulation of carboxylate species can cause atomic carbon formation on alumina acidic sites, but do not significantly impact catalyst deactivation.[97] If significant accumulation of carboxylic species in addition takes place on the neighbouring iron oxide phase, steric hindrance may affect the access of syngas to the active sites (diffusion limitations) and hence decreasing catalyst activity.[3]

Figure 13. Suggested routes for the formation of hydrocarbon and formate/carboxylate species on Fe-Cu/Al2O3 catalysts during FTS.

Conclusions

Iron-based catalysts (15 wt% of Fe) supported on alumina promoted with copper (0, 0.6, 2 and 5 wt% of Cu) were characterised in situ at relevant FTS conditions. The Fe2O3 precursor supported on γ-Al2O3 is undergoing a phase transition to Fe3O4 and subsequently to Fe5C2 (Hägg carbide) on Fe-Cu promoted catalysts during FTS. Cu favoured the fragmentation and carburization of Fe3O4 into smaller Fe5C2 nanoparticles (~ 10-30 nm) during FTS at higher temperatures (i.e. 280°C). Several catalyst features were enhanced by Cu promotion such as iron dispersion and reducibility via the H2/CO spillover effect from metallic Cu to iron oxide to form Hägg carbide. Intimate contact between Cu and Fe was necessary to bolster the formation of Fe5C2 nanoparticles. Iron-alumina support interactions are weakened by the addition of Cu, facilitating iron carburization and improving catalytic performance. Higher Cu loading leads to higher CO conversion, higher WGS activity, comparable hydrocarbon selectivities and lower O/P ratios due to higher hydrogenation activity. Approximately 20-22 % of the Fe in the catalysts with 2 and 5 wt% Cu were transformed into Hägg carbide. Increasing the Cu loading from 2 to 5 wt% did not further increase the iron carbide formation in the catalysts. Methylene species from wax-product and oxygenate species such as formate and carboxylate/carbonate were identified on the catalysts surface using in situ DRIFTS. Aliphatic hydrocarbons, formate and carboxylate species were detected on the catalyst surface during FTS. After exposing the spent catalysts to hydrogenation conditions, the carboxylate species remain strongly adsorbed while aliphatic hydrocarbons and formate species disappear. The accumulation of oxygenates species on the catalyst surface increased with Cu loading. The interaction of oxygenates with alumina and iron oxide particles (FexOy) were revealed, with the latter being a possible reason for inhibiting further iron carburization.

Acknowledgements

Keywords: Fischer-Tropsch synthesis; in situ characterization; carbide formation; copper promotion; oxygenated compounds

References:

[1]   D. Leckel. Energy & Fuels 2009, 23, 2342-2358.

[2]   J. van de Loosdrecht, F.G. Botes, I.M. Ciobîcă, A. Ferreira, P. Gibson, D.J. Moodley, A.M. Saib, J.L. Visagie, C.J. Weststrate, J.H. Niemantsverdriet. Comprehensive Inorg. Chem. II 2013, 7, 525-557.

[3]   D. Peña. Identification of deactivation mechanisms of cobalt Fischer-Tropsch catalysts in Slurry reactor 2013, PhD thesis, University of Lille 1.

[4]   P.K. Swain, L.M. Das, S.N. Naik. Renew. Sustain. Energy Rev. 2011, 15, 4917-4933.

[5]   G. Evans, C. Smith. Comprehensive Renew. Energy 2012, 5, 155-197.

[6]   B. Bao, M.M. El-Halwagi, N.O. Elbashir, Fuel Process Technol. 2010, 91, 703-713.

[7]   J. van Schijndel, N. Thijssen, G. Baak, A. Avhale, J. Ellepola, J. Grievink. 21 st Euro. Sym. Comp. Aided Process Eng. ESCAPE 2011, 21, 417-421.

[8]   V.S. Arutyunov, V.I. Savchenko, I.V. Sedov, I.G. Fokin, A.V. Nikitin, L.N. Strekova. Chem. Eng. J. 2015, 282, 206-212.

[9]   S. Srinivas, R.K. Malik, S.M. Mahajani. Energy Sustain. Dev. 2007, 11, 66-71.

[10]   A.Y. Khodakov, W. Chu, P. Fongarland. Chem. Rev. 2007, 107, 1692-1744.

[11]   C.-S. Chen, W.-H. Cheng, S.-S. Lin. Appl. Catal. A: Gen. 2004, 257, 97-106.

[12]   M. Martinelli, C.G. Visconti, L. Lietti, P. Forzatti, C. Bassano, P. Deiana. Catal. Today. 228 (2014) 77-88

[13]   T. Herranz, S. Rojas, F.J. Pérez-Alonso, M. Ojeda, P. Terreros, J.L.G. Fierro. Appl. Catal. A: Gen. 311 (2006) 66-75.

[14]   E. de Smit, F. Cinquini, A.M. Beale O. V. Safonova, W. van Beek, P. Sautet, B.M. Weckhuysen. J. Am. Chem. Soc. 132 (2010) 14928-14941.

[15]   N. Pour, M.R. Housaindokht, S.F. Tayyari, J. Zarkesh. J. Nat. Gas. Chem. 2010, 19, 362-368.

[16]   E. de Smit E, A.M. Beale, S. Nikitenko, B.M. Weckhuysen. J. Catal. 2009, 262, 244-256.

[17]   J.F. Bengoa, A.M. Alvarez, M.V. Cagnoli, N.G. Gallegos, S.G. Marchetti. Appl Catal A Gen. 2007, 325, 68-75.

[18]   T. Herranz, S. Rojas, F.J. Pérez-Alonso, M. Ojeda, P. Terreros, J.L.G. Fierro. J. Catal. 2006, 243, 199-211.

[19]   W. Ning, N. Koizumi, H. Chang, T. Mochizuki, T. Itoh, M. Yamada. Appl. Catal. A: Gen. 2006, 312, 35-44.

[20]   F.J. Pérez-Alonso, M. Ojeda, T. Herranz, S. Rojas, J.M. González-Carballo, P. Terreros, J.L.G. Fierro. Catal. Commun. 2008, 9, 1945-1948.

[21]   D.M. Shroff, D.S. Kalakkad, K.E. Coulter, S.D. Köhler, M.S. Harrington, N.B. Jackson A.G. Sault, and A.K. Datye. J. Catal. (1995) 156 185-207.

[22]   E. de Smit , B.M. Weckhuysen. Chem. Soc. Rev. 2008, 37, 2758-2781.

[23]   A.N. Pour, M.R. Housaindokht, J. Zarkesh, S.F. Tayyari. J. Ind. Eng. Chem. 2010, 16, 1025-1032.

[24]   A.N. Pour, S.M.K. Shahri, Y. Zamani, M. Irani, S. Tehrani. J. Nat. Gas. Chem. 2008, 17, 242-248.

[25]   A.N. Pour, M.R. Housaindokht, S.F. Tayyari, J. Zarkesh. J. Nat. Gas.Chem. 2010,19, 333-340.

[26]   Y. Jin Y, A.K. Datye. J. Catal. 2000, 196, 8-17.

[27]   Y. Zhang Y, N. Sirimanothan, R.J. O'Brien, H.H. Hamdeh, B.H. Davis. Stud. Surf. Sci. Catal. 2001, 139, 125-132.

[28]   S. Li, R.J. O'Brien, G.D. Meitzner, H. Hamdeh, B.H, Davis, E. Iglesia. Appl. Catal. A: Gen. 2001, 219, 215-222.

[29]   A.N. Pour, M.R. Housaindokht, S.F. Tayyari, J. Zarkesh, M.R. Alaei. J. Mol. Catal. A: Chem. 2010, 330, 112-120.

[30]   T. Herranz, S. Rojas, F.J. Pérez-Alonso, M. Ojeda, P. Terreros, J.L.G. Fierro. Appl. Catal. A: Gen. 2006, 308, 19-30.

[31]   H.-J. Wan, B.-S. Wu, C.-H. Zhang, H.-W. Xiang, Y.-W. Li, B.-F. Xu, F. Yi. Catal. Commun. 2007, 8, 1538-1545.

[32]   H.-J. Wan, B.-S. Wu, X. An, T.-Z. Li, Z.-C. Tao, H.-W. Xiang, Y.-W. Li. J. Nat. Gas Chem. 2007, 16, 130-138.

[33]   H.-j. WAN, B.-s. WU, T.-z. LI, Z.-c. TAO, X. AN, H.-w. XIANG, Y.-w. LI. J. Fuel Chem. Technol. 2007, 35, 589-594.

[34]   A.C.J. Koeken, H.M. Torres Galvis, T. Davidian, M. Ruitenbeek, K.P. de Jong. Angew. Chemie 2012, 124, 7302-7305.

[35]   M.V. Cagnoli, S.G. Marchetti, N.G. Gallegos, A.M. Alvarez, R.C. Mercader, A.A. Yeramian. J. Catal. 1990, 123, 21-30.

[36]   S.K. Das, S. Majhi, P. Mohanty, K.K. Pant. Fuel Process Technol. 2014, 118, 82-89.

[37]   H.-J. Wan, B.-S. Wu, Z-C. Tao, T.-Z. Li, X. An, H.-W. Xiang, Y.-W. Li. J. Mol. Catal. A Chem. 2006, 260, 255-263.

[38]   M. Luo, B.H. Davis. Stud. Surf. Sci. Catal. 2001, 139, 125-132.

[39]   S. Alayoglu, S.K. Beaumont, G. Melaet, A.E. Lindeman, N. Musselwhite, C.J. Brooks, M.A. Marcus, J. Guo, Z. Liu, N.Kruse, G. A. Somorjai. J. Phys. Chem. C. 2013, 117, 21803–21809.

[40]   C. Zhang, B.Teng, Y. Yang, Z. Tao, Q. Hao, H. Wan, F. Yi , B. Xu, H. Xiang, Y.Li. J. Mol. Catal. A: Chem. 2005, 239, 15-21.

[41]   G. Jacobs, W. Ma, P. Gao, B. Todic, T. Bhatelia, D.B. Bukur, B.H. Davis. Catal. Today 2013, 214, 100-139.

[42]   A. Voronov, A. Urakawa, W. van Beek, N.E. Tsakoumis, H. Emerich,   M. Rønning. Anal. Chim. Acta 2014, 840, 20-27.

[43]   E. Groppo, C. Prestipino, F. Cesano, F. Bonino, S. Bordiga, C. Lamberti, P.C. Thüne, J.W. Niemantsverdriet, A. Zecchina. J. Catal. 2005, 230, 98-108.

[44]   C. Wan, X. Ju, Y. Qi, Y. Xin, J. Qiu, S. Wang, X. Liu, L. Jiang. Int. J. Hydro. Energy 2010, 35, 2915–2920.

[45]   S. Pattanaika, G.P. Huffman, S. Sahu, R.J. Lee. Cem. Conc. Research 2004, 34, 1243-1249.

[46]   M.C. Ribeiro, G. Jacobs, R. Pendyala, B.H. Davis, D.C. Cronauer, A.J. Kropf, C.L. Marshall. J. Phys. Chem. C. 2011, 115, 4783-4792.

[47]   M.C. Ribeiro, G. Jacobs, B.H. Davis, D.C. Cronauer, A.J. Kropf, C.L. Marshall. J. Phys. Chem. C. 2010, 114, 7895-7903.

[48]   Y. Yang, C.A. Mims, R.S. Disselkamp, J.-H. Kwak, C.H.F. Peden, C.T. Campbell. J. Phys. Chem. C. 2010, 114 17205-17211.

[49]   Y. Yang, C. Mims C, R.S. Disselkamp, C.H.F. Peden, C.T. Campbell. Top. Catal. 2009, 52, 1440-1447.

[50]   J. Wang, V.F. Kispersky, W.N. Delgass, F.H. Ribeiro. J. Catal. 2012, 289, 171-178.

[51]   F.C. Meunier, D. Reid , A. Goguet, S. Shekhtman, C. Hardacre, R. Burch ,W. Deng, M. Flytzani-Stephanopoulos . J. Catal. 2007, 247, 269-279.

[52]   F.C. Meunier , A. Goguet , C. Hardacre, R. Burch, D. Thompsett. J. Catal. 2007, 252, 18-22.

[53]   A. Paredes-Nunez, D. Lorito, N. Guilhaume, C. Mirodatos, Y. Schuurman, F.C. Meunier. Catal. Today. 2014, 242, 178-183.

[54]   W. Rachmady, M.A. Vannice. J. Catal. 2002, 208, 158-169.

[55]   A.-M. Hilmen, E. Bergene, O.A. Lindvåg, D. Schanke, S. Eri, A. Holmen. Catal, Today. 2005, 105, 357-361.

[56]   Ø. Borg, S. Eri, E.A. Blekkan, S. Storsæter, H. Wigum, E. Rytter, A. Holmen. J. Catal. 2007, 248, 89-100.

[57]   A. Voronov, N.E. Tsakoumis, N. Hammer, W. van Beek, H. Emerich, M. Rønning. Catal. Today 2014, 229, 23-33.

[58]   N.E. Tsakoumis, R. Dehghan-Niri, M. Rønning, J.C. Walmsley, Ø. Borg, E. Rytter, A. Holmen. Appl. Catal. A: Gen. 2014, 479, 59-69.

[59]   N.E. Tsakoumis, A. Voronov, M. Rønning, W. van Beek, Ø. Borg, E. Rytter, A. Holmen. J. Catal. 2012, 291, 138-148.

[60]   N.E. Tsakoumis, R. Dehghan, R.E. Johnsen, A. Voronov, W. van Beek, J.C. Walmsley, Ø. Borg, E. Rytter, D. Chen, M. Rønning, A Holmen. Catal. Today 2013, 205, 86-93.

[61]   J.-D. Grunwaldt, M. Caravati, S. Hannemann and A. Baiker. Phys. Chem. Chem. Phys. 2004, 6, 3037-3047.

[62]   B. Ravel, M. Newville. J. Synchrotron Rad. 2005, 12, 537-541.

[63]   H. Li, M. Rivallan, F. Thibault-Starzyk, A. Travert F.C. Meunier. Phys. Chem. Chem. Phys. 2013, 15, 7321-7327.

[64]   N.E. Tsakoumis, A.P.E. York, D. Chen, M. Rønning. Catal. Sci. Technol. 2015.

[65]   L.A. Cano, A.A. Garcia Blanco, G. Lener, S.C. Marchetti, K. Sapag. Catal. Today 2017, 282, 204-213.

[66]   A.J.H.M. Kock, H.M. Fortuin, J.W. Geus. J. Catal. 1985, 96, 261-275.

[67]   R.J. O'Brien, B.H. Davis. Catal. Letters 2004, 94, 1-6.

[68]   V. Ramana, R. Pendyala, G. Jacobs, D.E. Sparks, S. Hopps, B.H. Davis BH. Catal. Letters 2014, 144, 1624-1635.

[69]   R.A. van Santen, I.M. Ciobîcă E. van Steen M.M. Ghouri. Ad. Catal. 2011, 54, 127-187.

[70]   V.A. de la Peña O'Shea, M.C. A lvarez-Galván, J.M. Campos-Martín, J.L.G. Fierro. Appl. Catal. A: Gen. 2007, 326, 65-73.

[71]   H. Schulz , M. Claeys. Appl. Catal. A: Gen. 1999, 186, 71-90

[72]   Z. Yan, Z. Wang, D.B. Bukur, D.W. Goodman. J. Catal. 2009, 268 196-200.

[73]   D.B. Bukur, X. Lang, A. Akgerman, Z. Feng. Ind. Eng. Chem. Res. 1997, 36, 2580–2587.

[74]   E. Iglesia, S.C. Reyes, R.J. Madon. J. Catal. 1991, 129, 238-256.

[75]   D.B. Bukur, X. Lang, Z. Feng. Texas A&M Univ. Dep. Chem. Eng. 1997, 43, 632-634.

[76]   D. Peña, A. Griboval-Constant, C. Lancelot, M. Quijada, N. Visez, O. Stéphan, V. Lecocq, F. Diehl, A.Y. Khodakov. Catal. Today. 2014, 228, 65-76.

[77]   S.-J. Park, J.W. Bae, Y.J. Lee, K.S. Ha, K.W. Jun, P. Karandikar. Catal. Commun. 2011, 12, 539-543.

[78]   D.B. Bukur, D. Mukesh, S.A. Patel. Ind. Eng. Chem. Res. 1990, 29 194-204.

[79]   G.B. Raupp, W.N. Delgass. J. Catal. 1979, 58, 348-360.

[80]   D. Peña. CATALIZADORES EN BASE A COBALTO EN LA SÍNTESIS FISCHER-TROPSCH 2007, Master thesis, Central University of Venezuela.

[81]   A. Espinosa, A. Serrano, A. Llavona, J. Jimenez de la Morena, M. Abuin, A. Figuerola, T. Pellegrino , J.F. Fernández , M. Garcia-Hernandez, G.R. Castro, M.A. Garcia. Meas. Sci. Technol. 2012, 23, 1- 6.

[82]   M. Lasfargues, Q. Geng, H. Cao, Y. Ding. Nanomaterials. 2015, 5, 1136-1146.

[83]   IRON OXIDE REDUCTION EQULIBRIA. Depart. Commerce Bureau of Mines. 1929, Bulletin 296, United States.

[84]   F. Hu, X. Wu, Y. Wang, X. Lai. RSC Adv. 2015, 5, 54053-54058.

[85]   T.P. Almeida, M.W. Fay, Y. Zhu, P.D. Brown. Phys. E 2012, 44, 1058-1061.

[86]   R. Kumar, S. Gautam, I.C. Hwang, J.R. Lee, K.H. Chae, N. Thakur. Mater. Lett. 2009, 63, 1047-1050.

[87]   Y.C. Dong, M.J. Hu, H. Cheng, Y.Y. Li, J.A. Zapien. Cryst. Eng. Comm. 2013, 15, 1324-1331.

[88]   S. Janbroersa, P.A. Crozier, H.W. Zandbergen, P.J. Kooyman. Appl. Catal. B: Environ. 2011, 102, 521-527.

[89]   S. Janbroers, J.N. Louwen, H.W. Zandbergen, P.J. Kooyman J. Catal. 2009, 268, 235-242.

[90]   M. Dirand, L. Afqir. Acta Metall. 1983, 31, 1089-1107.

[91]   X. Zhou, J. Ji, Di Wang, X. Duan, G. Qian, D. Chen, X. Zhou. Chem. Commun. 2015, 51, 8853-8856.

[92]   D. Bianchi, T. Chafik, M. Khalfallah, S.J. Teichner. Appl. Catal. A: Gen. 1995, 123, 89-110.

[93]   D. Lorito, A. Paredes-Nunez, C. Mirodatos, Y. Schuurman, F.C. Meunier. Catal. Today 2016, 259, 192-196.

[94]   F.C. Meunier. React. Chem. Eng. 2016, 1, 134-141.

[95]   K. Arouri, P.F. Greenwood, M.R. Walter. Org, Geochem. 1999, 30, 1323-1337.

[96]   F.C. Meunier, J.P. Breen, V. Zuzaniuk, M. Olsson, J.R.H. Ross. J. Catal. 1999, 187, 493-505.

[97]   D. Kistamurthy, A.M. Saib, D.J. Moodley, H. Prestona, I.M. Ciobîcǎ, W. Janse van Rensburg, J.W. Niemantsverdriet, C.J. Weststratec. Catal. Today. 2015, 275, 127-134.

[98]   E. de Smit, M.M. van Schooneveld, F. Cinquini, H. Bluhm, P. Sautet, F.M.F. de Groot, B.M. Weckhuysen. Angew. Chemie. Int. Ed. 2011, 50, 1584-1588.

[99]   R. Valdez, D.B. Grotjahn, D.K. Smith, J.M. Quintana, A. Olivas. Int. J. Electrochem Sci. 2015, 10, 909-918.

[100]   M. Fathi, A.A. Entezami. Surf. Interface Anal. 2014, 46, 145-151.

[101]   K. Cheng, N.A. Frey, S. Sun, S. Peng, K. Cheng, S. Sun. Chem. Soc. Rev. 2009, 38, 2532-2542.

[102]   J. Govan, Y. Gun'ko. Nanomaterials. 2014, 4, 222-241.

[103]   P.C.A. Bruijnincx, G. van Koten, R.J.M. Klein Gebbink. Chem. Soc Rev. 2008, 37, 2716-2744.